Journal of the Mechanics and Physics of Solids (2011)
in press

Experimental evidence of flutter and divergence instabilities induced by dry friction

Davide Bigoni* and Giovanni Noselli

Department of Mechanical and Structural Engineering, University of Trento
via Mesiano 77, Trento, Italy

Abstract

Flutter and divergence instabilities have been advocated to be possible in elastic structures with Coulomb friction, but no direct experimental evidence has ever been provided. Moreover, the same types of instability can be induced by tangential follower forces, but these are commonly thought to be of extremely difficult, if not impossible, practical realization. Therefore, a clear experimental basis for flutter and divergence induced by friction or follower-loading is still lacking. This is provided for the first time in the present article, showing how a follower force of tangential type can be realized via Coulomb friction and how this, in full agreement with the theory, can induce a blowing-up vibrational motion of increasing amplitude (flutter) or an exponentially growing motion (divergence). In addition, our results show the limits of a treatment based on the linearized equations, so that nonlinearities yield the initial blowing-up vibration of flutter to reach eventually a steady-state. The presented results give full evidence to potential problems in the design of mechanical systems subject to friction, open a new perspective in the realization of follower loading systems and of innovative structures exhibiting 'unusual' dynamical behaviours.

Keywords: Coulomb friction; flutter instability; divergence instability; follower load

1 Introduction

Coulomb friction at the contact between two elastic bodies is an example of a live load (since it acts in a direction opposite to the relative velocity during sliding of the bodies) and is known to be connected to different forms of instabilities. Two of these, the so-called 'flutter' and 'divergence' (the former associated to blowing-up oscillations and the latter to an exponentially growing motion), are dynamical instabilities that have been *theoretically* shown to be possible in elastic structural systems with Coulomb friction (Martins et al., 1999; Simões and Martins, 1998; Nguyen, 2003) and even in plastic continua characterized by frictional behaviour (Rice, 1977; Loret, 1992; Bigoni, 1995; Bigoni and Loret, 1999; Loret et al., 2000; Piccolroaz et al., 2006). However, *no clear experimental evidence of flutter and divergence instabilities related to dry friction has ever been presented* [1], so

*Corresponding author: e-mail: bigoni@ing.unitn.it; phone: +39 0461 282507.

[1] Friction-related dynamical instabilities are thought to be responsible of brake squeal and of the 'song' of a fingertip moved upon the rim of a glass of water, but these phenomena involve stick and slip, a phenomenon modelled as a drop of friction coefficient with velocity (Rice and Ruina, 1983). It is therefore not clear if the instabilities would occur in the absence of this drop and it is not possible to definitely conclude about the real nature of these, which appear to be only weakly related to the flutter of the structures subject to follower load, so that there are many different theories to describe brake squeal involving or not follower forces (see the reviews by Flint and Hultén, 2002; Kröger et al., 2008).

that flutter induced by friction has always been thought to be a puzzling phenomenon, since it is rather 'unexpected' that a merely dissipative factor such as friction, can induce blowing-up dynamical motions in a mechanical system that would be stable in the absence of it. Moreover, for friction-related flutter in structures and continua, the role played by the nonlinearities, usually neglected in the stability analyses, is simply not known from the experimental point of view, so that these could even have a stabilizing effect, see the discussion by Bigoni and Petryk (2002).

The primary purpose of this article is to provide a definitive and indisputable experimental evidence for flutter and divergence instability in elastic systems with dry Coulomb friction. The key for this achievement is the link with a special elastic structure exhibiting flutter and divergence: the so-called 'Ziegler column' (Ziegler, 1953; 1977). This is a two-degree-of-freedom structure made up of two rigid bars, internaly jointed with an elastic rotational spring, externally fixed at one end through another elastic rotational spring, while at the other end subject to a tangential follower load, remaining coaxial to the rod to which it is applied, Fig. 1. Since the follower load is nonconservative, the

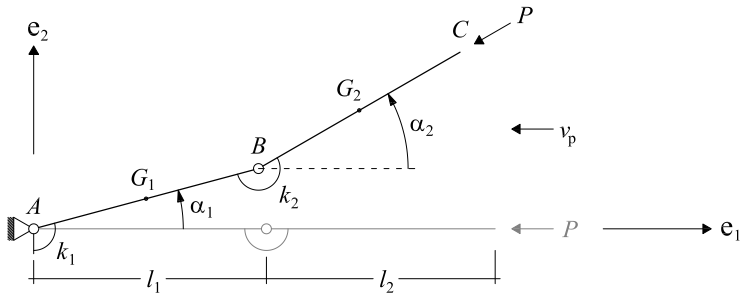

Fig. 1: The Ziegler column, a two-degree-of-freedom system subject to follower load (the force **P** remains always applied to C and directed parallel to the rod BC), exhibiting flutter and divergence instability. The two rods, of linear mass density ρ, are rigid and connected through two rotational springs of stiffness k_1 and k_2. Note that there is no bifurcation for this system.

structure becomes dynamically unstable at a certain load level (although non-trivial equilibrium configurations do not exist), so that it evidences flutter (a blowing-up oscillating motion) and, at higher load, divergence instability (an exponentially growing motion) [2] .

As a result of a complex fluid-structure interaction, follower loads and related instabilities may occur in aeroelasticity, but these do not directly involve the tangential follower force postulated in the Ziegler column, which is thought to be of such difficult practical realization[3] that a clear experimental basis for flutter and divergence instability as induced by tangential follower load is still lacking. These difficulties led Professor W.T. Koiter (1996) to propose the 'elimination of the abstraction of follower forces as external loads from the physical and engineering literature on elastic stability' and to conclude with the warning: 'beware of unrealistic follower forces'.

In the present article we show that it is possible to exploit dry friction to generate follower loads of

[2]The history of the discovery of this instability involves, among others, Nikolai (1928), Pflüger (1950; 1955), Beck (1952), Ziegler (1953; 1956; 1977), Bolotin (1963), Herrmann and Jong (1965), Como (1966) and is explained in detail by Elishakoff (2005), who also provides an account of the frustrating attempts of giving experimental evidence to the theory.

[3]Follower tangential forces have been realized until now through a fluid flowing from a nozzle, or through a solid motor rocket fixed at the end of the structure (Herrmann et al., 1966; Sugiyama et al., 1995; 2000), two devices introducing complications in the modelling. In fact, the complex fluid/structure interaction of a fluid flowing from a nozzle is only as a first approximation reduced to a follower thrust, while in the other experimental set-up complications arise from the non-negligible mass and dimensions of the solid motor rocket and from the short duration of the thrust provided by it, which prevents long-term analyses of the motion.

the type postulated by Ziegler (1953; 1977), so that flutter and divergence instabilities in structures and in mechanical systems with dry friction are shown to be strictly connected phenomena. In particular, we will prove the following results.

- First, we definitely disclaim Koiter's statement and the current opinion that follower forces are unrealistic, showing that *a follower load can be easily realized exploiting dry friction and that flutter and divergence instabilities can be observed with a simple experimental setting, so simple that can even be reduced to a toy for kids.*
- Second, *we prove in a direct and indisputable way that flutter and divergence instabilities can be induced by dry friction.*
- Third, *we investigate experimentally and theoretically the role of nonlinearities on the development of the instability, showing that in the case of flutter these induce the attainment of a steady-state motion.*

The above mentioned results have been obtained by inventing, designing and testing a two-degree-of-freedom elastic structure with a frictional (obeying the Coulomb rule) element.

A brief explanation of our idea and results can be given as follows. Our two-degree-of-freedom system is a simple variant to the Ziegler column (Fig. 1), where the follower load is induced by a frictional force acting on a wheel mounted at the end of the structure and kept sliding with friction against a plane. Note the crucial role played by the wheel, which transmits the frictional force coaxial to its axis (see the sketch in Fig. 3). The behaviour of the structure is shown in Fig. 2, where photos taken at different time instants have been superimposed. On the left of the figure we may see an

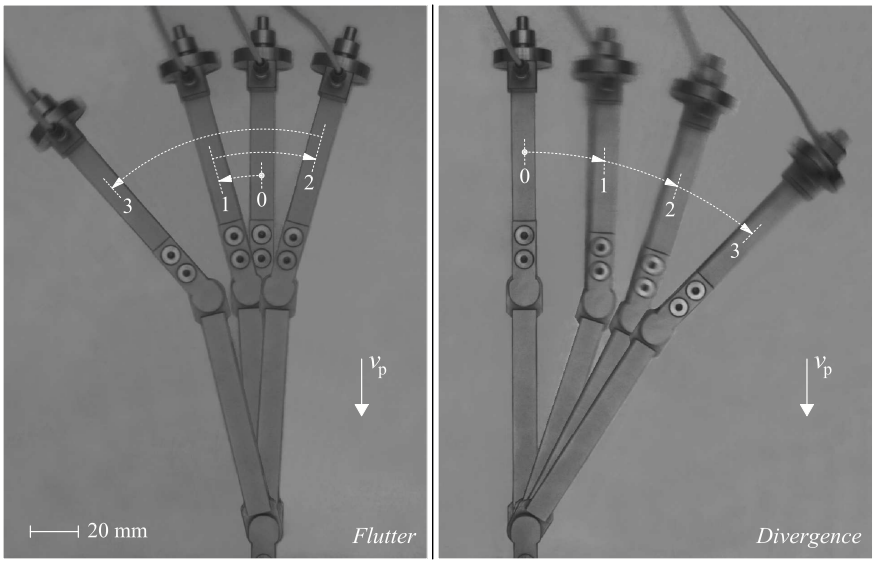

Fig. 2: A superposition of photos, adapted from Figs. 10 and 14 on the left, taken at different instants of time [(0, 0.48, 0.72, 1.08) s for flutter and (0, 0.20, 0.28, 0.36) s for divergence] of the two-degree-of-freedom structure (Fig. 8b) exhibiting flutter (left) and divergence (right) instability. v_p is the velocity of a plate sliding against the wheel, taken equal to 75 mm/s for flutter and 50 mm/s for divergence.

example of flutter instability, while on the right an example of divergence. The numbers provide the order in which the photos have been taken, so that we can clearly detect the oscillatory blow-up of

flutter, to be contrasted with the progressive growth of divergence[4] .

The article is organized as follows. A variant of the Ziegler column is presented in Section 2, in which the mass is distributed along the two rigid beams forming the system and the follower load is provided by a frictional device obeying Coulomb friction. The basic ideas for the design of the structure and the complication involved with the friction constraint are detailed. The practical realization of the structure is described in Section 3, where experimental results are provided and commented. A final discussion closes the article, Section 4.

2 The two-degree-of-freedom system

It is well-known that flutter instability may be induced in a structure by follower loads and the typical example is the so-called 'Ziegler column', the two-degree-of-freedom system with heavy rigid rods (mass per unit length ρ) shown in Fig. 1, where two rotational springs of stiffness k_1 and k_2 provide the elasticity. The generic configuration of the structure remains determined by the two Lagrangean parameters α_1 and α_2. The applied load $\mathbf{P}$, assumed positive when compressive, maintains the direction parallel to the rod BC. The analysis of a system similar to this (with concentrated masses instead than diffused) can be found in Herrmann (1971), Ziegler (1977) and, in a simplified version, in Nguyen (1995), while the analogous problem of a clamped column subjected to a load tangential to its axis at the free end has been solved by Beck (1952) and Pflüger (1955).

The follower force $\mathbf{P}$ in the structure shown in Fig. 1 has been previously realized through a fluid flowing from a nozzle (Herrmann et al., 1966) or through an end rocket (Sugiyama et al., 1995; 2000) fixed at the end of the structure. Our idea is

> *to provide the follower force through a wheel of negligible mass mounted at the top of the structure and constrained to slide against a frictional plane, see Fig. 3.*

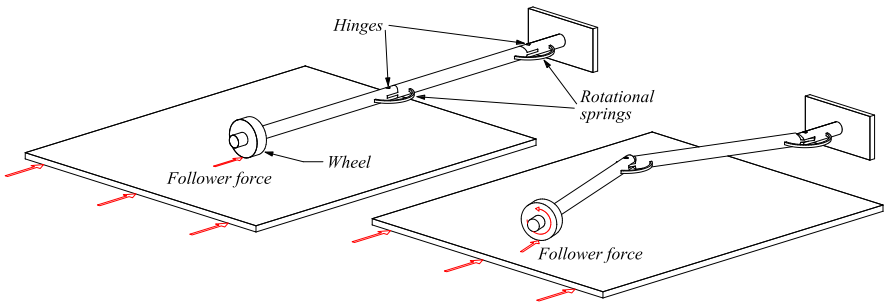

Fig. 3: The way to produce a force coaxial to a rod from friction; a freely rotating wheel of negligible mass is mounted at the top of the rod.

In fact, a perfect (massless and fully free of rotating) wheel sliding with pure Coulomb friction (but without rolling friction) on a rigid plane, which is ideally touched at a point, can only transmit an axial force and we will show that these conditions can be successfully approximated in real experiments, since the deviations from the ideal model that necessarily arise in experiments are not sufficient to hide the instabilities.

[4] A movie with experiments can be downloaded at http://ssmg.ing.unitn.it/. Note in the movie the acoustic emission during the test, also evidencing the instability.

Following the above-mentioned idea, we analyze the structure shown in Fig. 1 under the hypotheses that: (i.) the wheel is massless, free of rotating, and touches the horizontal plane at a point, (ii.) the hinges (unloaded in the straight configuration) are viscoelastic, (iii.) the follower force is transmitted through Coulomb friction of coefficient μ_d by a plane moving at the speed $-v_p\,\mathbf{e}_1$, and that (iv.) there is no rolling friction, so that the analysis merely differs from results in the above-mentioned literature in the inclusion of the friction condition at the end of the structure.

The above-mentioned assumptions (i.)–(iv.) are very close to our experimental setup and have been verified both experimentally (changing the wheel's mass and profile, the friction coefficient, the geometry of the structure and the stiffness and viscosity of the springs, see Section 3) and theoretically (we have performed more sophisticated computations by introducing the mass and rotational inertia of the wheel, the rolling friction and a possible deviation of the frictional load from collinearity), so that we may point out that, though more complex models might yield a better quantitative comparison with experiments, they cannot change the overall qualitative picture, which will be shown to be very well captured with simple assumptions.

A simple static analysis of the structure shown in Fig. 1 is sufficient to conclude that only the trivial (straight) configuration satisfies equilibrium (in fact equilibrium of the rod BC is only possible if $\alpha_1 = \alpha_2$, while equilibrium of the complex ABC requires $\alpha_1 = 0$), so that bifurcations are excluded.

Let us obtain now the equations of motion for the system. To this purpose, we start from the position vectors of the point $\mathbf{C}$ and of the mass center of the rods $\mathbf{G}_1$ and $\mathbf{G}_2$

$$\begin{aligned}
\mathbf{C}-\mathbf{A} &= (l_1\cos\alpha_1 + l_2\cos\alpha_2)\mathbf{e}_1 + (l_1\sin\alpha_1 + l_2\sin\alpha_2)\mathbf{e}_2,\\
\mathbf{G}_1-\mathbf{A} &= [(l_1/2)\cos\alpha_1]\mathbf{e}_1 + [(l_1/2)\sin\alpha_1]\mathbf{e}_2,\\
\mathbf{G}_2-\mathbf{A} &= [l_1\cos\alpha_1 + (l_2/2)\cos\alpha_2]\mathbf{e}_1 + [l_1\sin\alpha_1 + (l_2/2)\sin\alpha_2]\mathbf{e}_2,
\end{aligned} \tag{1}$$

where $\mathbf{e}_1$ and $\mathbf{e}_2$ are the two unit vectors singling out the horizontal and vertical direction respectively, so that the follower force $\mathbf{P}$, of modulus P, can be expressed as

$$\mathbf{P} = -P\,\mathbf{e}_1\,\cos\alpha_2 - P\,\mathbf{e}_2\,\sin\alpha_2, \tag{2}$$

where, denoting with a superimposed dot the derivative with respect to time, P is given by the Coulomb friction law with stiction

$$P = R\,\mu(\dot{C}_p^r), \quad \mu(\dot{C}_p^r) = \begin{cases} \mu_d\,\mathrm{sign}(\dot{C}_p^r), & \text{if } \dot{C}_p^r = \dot{\mathbf{C}}_p\cdot\mathbf{e}_r \neq 0,\\ [-\mu_s,\ \mu_s], & \text{if } \dot{C}_p^r = \dot{\mathbf{C}}_p\cdot\mathbf{e}_r = 0, \end{cases} \tag{3}$$

where R is the vertical reaction applied at the wheel (orthogonal to the moving plane), μ_s and μ_d are the static and dynamic friction coefficients (their difference gives the 'stiction effect', which vanishes taking $\mu_s = \mu_d$) and $\dot{C}_p^r$ is the radial component ($\mathbf{e}_r = \cos\alpha_2\,\mathbf{e}_1 + \sin\alpha_2\,\mathbf{e}_2$) of the velocity of the wheel relative to the plate, so that we can write

$$\dot{\mathbf{C}}_p = \dot{\mathbf{C}} + v_p\,\mathbf{e}_1, \qquad \dot{\mathbf{C}}_p\cdot\mathbf{e}_r = v_p\,\cos\alpha_2 - l_1\sin(\alpha_1-\alpha_2)\dot{\alpha}_1. \tag{4}$$

For the practical realization of the experiment, the vertical reaction R will be provided by using the structure itself as a lever to which a dead load W is applied, as sketched in Fig. 4, so that

$$R = \frac{l_s}{l_f + l_1\cos\alpha_1 + l_2\cos\alpha_2}\,W, \tag{5}$$

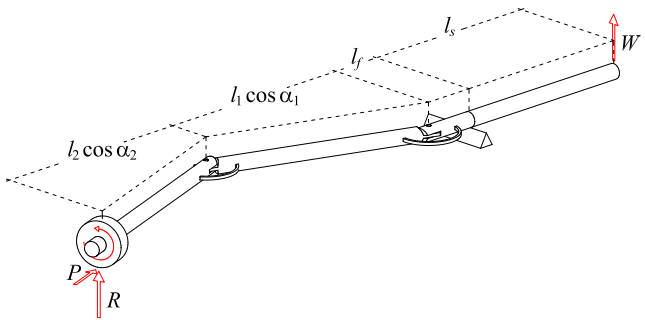

Fig. 4: The structure shown in Fig. 3 is used as a lever to provide the vertical reaction R from the vertical dead load W, so that the force from friction results $P = \mu_d R$.

where l_s is the length of one arm of the lever, while the denominator is the variable length of the other, see Fig. 4.

It is assumed that the hinges are viscoelastic of the Voigt type with constants β_1, β_2, k_1, and k_2, so that the moments applied to the rods are $k_1\alpha_1 + \beta_1\dot{\alpha}_1$ and $k_2(\alpha_2 - \alpha_1) + \beta_2(\dot{\alpha}_2 - \dot{\alpha}_1)$ and the principle of virtual works, denoting with '$\cdot$' the scalar product, writes as (see Appendix A for details)

$$\begin{aligned} \delta W \;=\; & \mathbf{P}\cdot\delta\mathbf{C} - (k_1\alpha_1 + \beta_1\dot{\alpha}_1)\delta\alpha_1 - [k_2(\alpha_2-\alpha_1) + \beta_2(\dot{\alpha}_2 - \dot{\alpha}_1)](\delta\alpha_2 - \delta\alpha_1) + \\ & -\rho l_1 \ddot{\mathbf{G}}_1 \cdot \delta\mathbf{G}_1 - \rho l_2 \ddot{\mathbf{G}}_2 \cdot \delta\mathbf{G}_2 - \frac{1}{12}\,\rho\, l_1^3\,\ddot{\alpha}_1\delta\alpha_1 - \frac{1}{12}\,\rho\, l_2^3\,\ddot{\alpha}_2\delta\alpha_2 = 0, \end{aligned} \tag{6}$$

holding for every virtual rotation $\delta\alpha_1$ and $\delta\alpha_2$. Imposing now the condition (6) and invoking the arbitrariness of $\delta\alpha_1$ and $\delta\alpha_2$ we arrive at the two nonlinear differential equations

$$\begin{cases} \dfrac{1}{3}\rho l_1^2\,(l_1 + 3l_2)\,\ddot{\alpha}_1 + \dfrac{1}{2}\rho l_1 l_2^2 \cos(\alpha_1-\alpha_2)\ddot{\alpha}_2 + \dfrac{1}{2}\rho l_1 l_2^2 \sin(\alpha_1-\alpha_2)\dot{\alpha}_2^2 + (k_1+k_2)\alpha_1 - k_2\alpha_2 + \\ +(\beta_1+\beta_2)\dot{\alpha}_1 - \beta_2\dot{\alpha}_2 - l_1 P(\dot{C}_p^r)\sin(\alpha_1-\alpha_2) = 0, \\ \dfrac{1}{2}\rho l_1 l_2^2 \cos(\alpha_1-\alpha_2)\ddot{\alpha}_1 + \dfrac{1}{3}\rho l_2^3\ddot{\alpha}_2 - \dfrac{1}{2}\rho l_1 l_2^2 \sin(\alpha_1-\alpha_2)\dot{\alpha}_1^2 - k_2(\alpha_1-\alpha_2) - \beta_2(\dot{\alpha}_1 - \dot{\alpha}_2) = 0, \end{cases} \tag{7}$$

governing the dynamics of the system. A numerical solution of the nonlinear differential system (7) faces the well-known numerical difficulty that the friction law (3) is a multivalued, discontinuous relation (Threlfall, 1977; Oden and Martins, 1985; Martins et al., 1990). This difficulty can be overcome using a viscous smooth approximation of the law, including or not the difference between static and dynamical friction, which in the continuous approximation becomes the so-called 'Stribeck effect' (Stribeck, 1902). In the following, we have numerically solved the system (7) using different approximations to the law (3), including and neglecting the Stribeck effect, and we have found that results *for our structure* do not differ much, so that the root of the unstable behaviour is *not* linked to a drop in the friction coefficient. Therefore, we will refer to the simple approximation to the relation (3) employed by Oden and Martins (1985) and Martins et al. (1990)

$$\mu(\dot{C}_p^r) = \mu_d \begin{cases} \operatorname{sign}(\dot{C}_p^r), & \text{if } \dot{C}_p^r \notin [-\varepsilon,\varepsilon], \\ \left(2 - \dfrac{|\dot{C}_p^r|}{\varepsilon}\right)\dfrac{\dot{C}_p^r}{\varepsilon}, & \text{if } \dot{C}_p^r \in [-\varepsilon,\varepsilon], \end{cases} \tag{8}$$

where ε is a small parameter.

A purely elastic analysis ($\beta_1 = \beta_2 = 0$) of the structure (a linear viscoelastic analysis is deferred to Appendix A), valid for configurations in a small neighborhood of the trivial one ($\alpha_1 = \alpha_2 = 0$) can be performed with the incrementally nonlinear differential system obtained from Eqs. (7) through a Taylor series expansion in the form

$$\begin{cases} \dfrac{1}{3}\rho l_1^2\,(l_1+3l_2)\,\ddot{\alpha}_1 + \dfrac{1}{2}\rho l_1 l_2^2\ddot{\alpha}_2 + (k_1+k_2)\alpha_1 - k_2\alpha_2 - l_1 P(\dot{C}_p^r)(\alpha_1-\alpha_2) = 0, \\ \dfrac{1}{2}\rho l_1 l_2^2\ddot{\alpha}_1 + \dfrac{1}{3}\rho l_2^3\ddot{\alpha}_2 - k_2(\alpha_1-\alpha_2) = 0, \end{cases} \tag{9}$$

where $P(\dot{C}_p^r)$ remains the incrementally nonlinear function (3). Note that the Eqs. (9) are similar (keeping aside for the moment the complication related to the difference between μ_s and μ_d) to the piecewise incremental nonlinearity of a rigid perfectly-plastic body. The complication connected to the incremental nonlinearity disappears if the plate/wheel sliding condition $\dot{C}_p^r > 0$ is always verified, a situation which certainly holds *at the instant* of flutter (when $\alpha_1 = \alpha_2 = 0$) and *even for a finite interval of time* from this instant, for v_p sufficiently high to satisfy $v_p > l_1 \sin(\alpha_1 - \alpha_2)\dot{\alpha}_1 / \cos\alpha_2$. In this case, we can operate with the fully linearized version of Eqs. (7)

$$\begin{cases} \dfrac{1}{3}\rho l_1^2\,(l_1+3l_2)\,\ddot{\alpha}_1 + \dfrac{1}{2}\rho l_1 l_2^2\ddot{\alpha}_2 + (k_1+k_2)\alpha_1 - k_2\alpha_2 - l_1 P(\alpha_1-\alpha_2) = 0, \\ \dfrac{1}{2}\rho l_1 l_2^2\ddot{\alpha}_1 + \dfrac{1}{3}\rho l_2^3\ddot{\alpha}_2 - k_2(\alpha_1-\alpha_2) = 0, \end{cases} \tag{10}$$

where P is now independent of $\dot{C}_p^r$ and given by

$$P = \mu_d\, R = \mu_d\, \frac{l_s}{l_f + l_1 + l_2}\, W. \tag{11}$$

In the flutter analyses usually performed in nonassociative elastoplasticity (see for instance Bigoni, 1995), 'plastic loading' is always assumed, in other words, a fully linear system such as that described by Eqs. (10) and (11) is considered. We will soon be in a position to test this assumption on our structure both theoretically and experimentally; for the moment, continuing with the linearization, Eq. (11), we look for time-harmonic vibrations so that we can conclude that (see Appendix A for details):

- *flutter instability* occurs when $W_f < W < W_d$, with

$$W_{\substack{f\\d}} = \frac{k_2(l_f+l_1+l_2)}{\mu_d l_s l_1} \cdot \frac{k + (1+\lambda)^3 \mp \lambda\sqrt{k(3+4\lambda)}}{1+3\lambda/2}, \tag{12}$$

  where $\lambda = l_1/l_2$ and $k = k_1/k_2$,

- and *divergence instability* occurs when $W > W_d$.

In addition to the above-reported calculations, we have analyzed the case (not presented for brevity) that the follower force slightly deviates from collinearity with the end rod. We have concluded that the model is robust with respect to this deviation, in the sense that a small deviation from collinearity does not suppress flutter and divergence instability.

The linearized analysis yields the known conclusion (which cannot be reached through a quasi-static analysis) that, *while divergence instability corresponds to a motion growing exponentially in*

time, flutter instability corresponds to a self-excited oscillation blowing-up in time. This statement is confirmed in Fig. 5, where results are reported as solution of the linear differential system (10) with the initial conditions $\alpha_1 = \alpha_2 = 0.5°$ ($\alpha_1 = \alpha_2 = -0.5°$ for divergence) and $\dot{\alpha}_1 = \dot{\alpha}_2 = 0$ and with the geometric and stiffness setting that will be employed for experiments (see Tab. 2). A 0.52

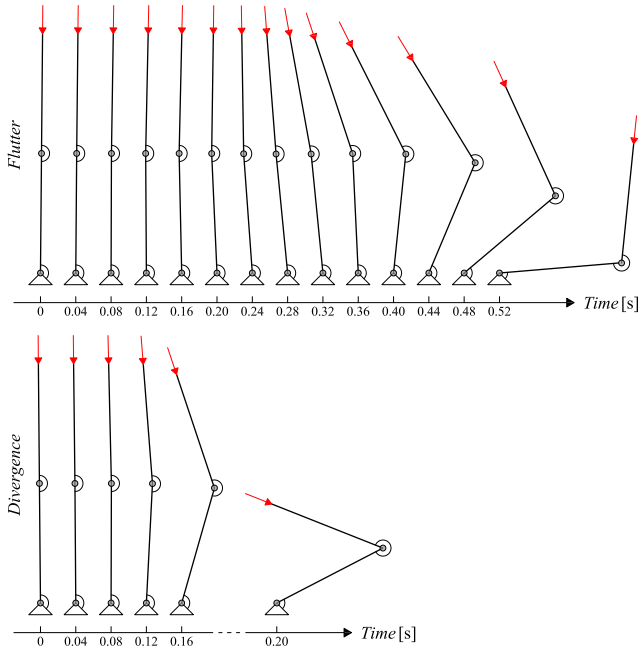

Fig. 5: A sequence (0.52 s for flutter and to 0.2 s for divergence) of deformed shapes at consecutive times intervals of 0.04 seconds of the structure sketched in Fig. 1 and exhibiting flutter (upper part) and divergence (lower part) instability. Results have been obtained through a linearized analysis [Eqs. (10)] with initial conditions $\alpha_1 = \alpha_2 = 0.5°$ ($\alpha_1 = \alpha_2 = -0.5°$ for divergence) and $\dot{\alpha}_1 = \dot{\alpha}_2 = 0$, at the flutter load $(W_f + W_d)/2$ (upper part) and at the divergence load $1.75\, W_d$ (lower part), Eq. (12). The values employed for the analysis are reported in Tab. 2.

(0.2) seconds sequence of configurations at different instants of time is reported in the figure, where each configuration is drawn at fixed intervals of time (0.04 s). The oscillatory blow-up (exponential growth) of the solution is clearly visible in the case of flutter (divergence).

The linearized elastic analysis has the mentioned limitations that: (i.) slip at the wheel/plate contact is assumed, $\dot{C}_p^r > 0$, (ii.) geometrical nonlinearities are neglected, and (iii.) viscous behaviour of the hinges is set to zero. So that the the question arises whether the blowing-up motion connected to flutter (or to divergence) really develops or is strongly altered, maybe even 'damped-down', by nonlinearities. We can provide various answers to these questions, which are now discussed in detail.

- Assumption (i.), namely, $\dot{C}_p^r > 0$. For sufficiently high velocities of the plate, v_p, this condition is verified not only at the instant of flutter, but also for a finite interval of time, say, until $l_1(\alpha_1 - \alpha_2)\dot{\alpha}_1$ remains sufficiently small when compared to v_p. It is therefore expected that *the linearized analysis based on Eqs. (10) correctly predicts the onset and the early development of a dynamical instability, without involving any stick-slip phenomena.* This statement is verified in the example reported in Fig. 5, where we have observed that the wheel/plate slip condition is satisfied for all reported configurations until the instant of time 0.40 s for flutter (0.16 s for divergence). Therefore, the problem to be addressed is not if flutter and divergences are 'true' instabilities, but how these instabilities develop when displacements become sufficiently large to

violate the wheel/plate slip condition (and to involve the other nonlinearities). This problem is solved in the following both with a numerical and an experimental approach.

- Assumptions (ii.). The geometrical nonlinearities play a role only when the displacement of the structure becomes large. These effects need to be included for a correct modelling of the experiments, since we have observed large (and very fast) movements to occur, so large in the case of divergence instability, that we have had to limit the maximum stroke of the structure with a constraint, to avoid failure of the equipment.

- Assumptions (iii.). We have experimentally detected (in a way independent of the instability tests, that will be explained later) a viscous behaviour of the hinges, the consideration of which in the modelling has yield a better comparison to experiments. In any case, the instability is not associated to the viscosity, so that we have observed it to occur under various conditions of lubrication at the hinges.

To check the limits of the above assumptions and to be able to model our experiments, we have provided fully nonlinear analyses of the differential system (7), employing the regularization (8) with $\varepsilon = 10^{-5}$ m/s. One of these analyses (performed numerically using the function 'NDSolve' of Mathematica 6.0) is shown in Fig. 6, where configurations at different instants of time have been reported as in Fig. 5, but introducing now also the damping coefficients β_1 and β_2, with the values that best fit our experiments (that will be introduced in the next Section, see Tabs. 1 and 2). We highlight

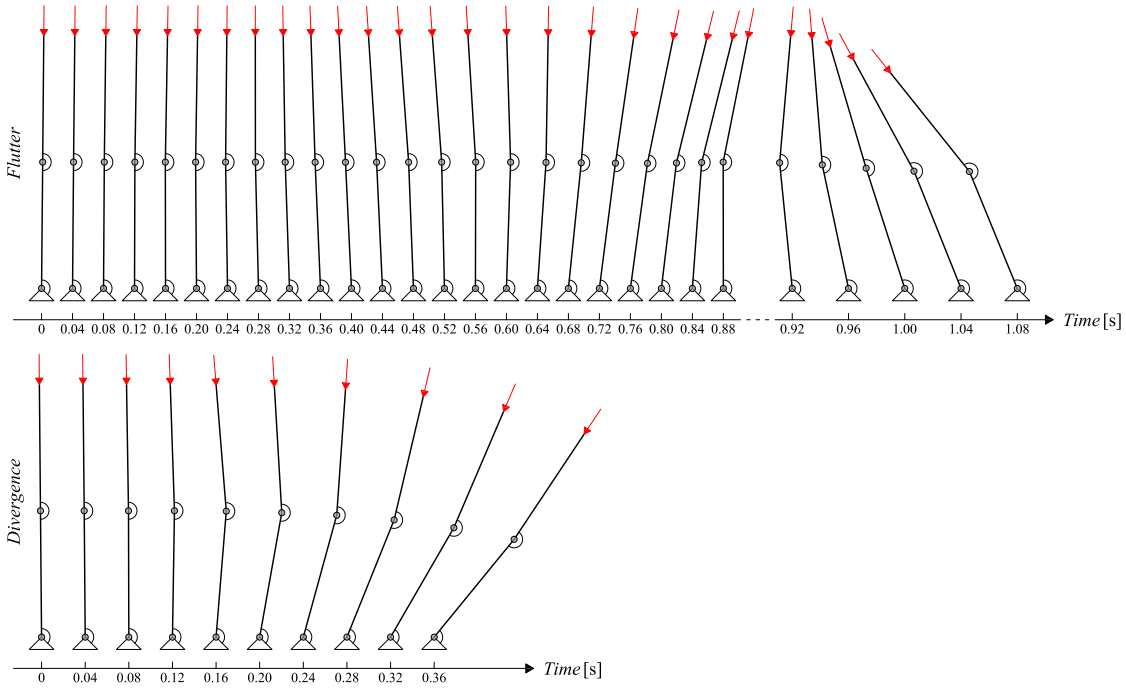

Fig. 6: A sequence (1.08 s for flutter and to 0.36 s for divergence) of deformed shapes at consecutive times intervals of 0.04 seconds of the structure sketched in Fig. 1 and exhibiting flutter (upper part) and divergence (lower part) instability. Results have been obtained through a numerical analysis of Eqs. (7) with initial conditions $\alpha_1 = \alpha_2 = 0.5^\circ$, at the flutter load $(W_f + W_d)/2$ (upper part) and at the divergence load $1.75\, W_d$ (lower part), Eq. (12). The values employed for the analysis are reported in Tab. 2.

that for all the deformed configurations reported in Fig. 6 for flutter, the regularization law (8) is not

'activated', so that $\dot{C}_p^r > \varepsilon$, while in the case of the divergence, the regularization is activated starting from the configuration at the instant of time 0.20 s. This means that in the conditions relevant for our experiments, the early development of flutter and divergence fully occurs *without* involving transitions from the dynamic to static friction coefficients, with the possibility of stick-slip instabilities.

We can conclude from Fig. 6 that an initial oscillation of increasing amplitude is observed, as would be predicted by a linearized analysis, but that *the oscillation becomes steady at large deformations* (see the electronic supplementary material and also http://ssmg.ing.unitn.it/), so large which could yield the failure of a real structure (in fact we have broken our first two prototypes of the structure during early tests, so that eventually we have designed the third prototype to resist large displacements). A plot of the movement of the tip of the structure recorded on the moving plate, as calculated from solution of the nonlinear Eqs. (7) is reported in Fig. 7, contrasted with an experimental result, namely, a scratch left on the plate by the wheel during a test (evidenced with red spots). Note that the initial velocity has been taken equal to $\dot{\alpha}_1 = \dot{\alpha}_2 = 0.5\,\mathrm{rad/s}$, since in the experiment we have observed first a slight deviation from rectilinearity and then a movement to reach the straight configuration before the initiation of flutter. We can observe that cusps form in the predicted behaviour when the steady motion is reached, a feature which is present also in the experiment and which is related with the decrease to zero of $\dot{C}_p^r$. We have found that the slip velocity $\dot{C}_p^r$ never became negative in all nonlinear simulations that we have performed. We have observed some of the scratches left by the wheel on the

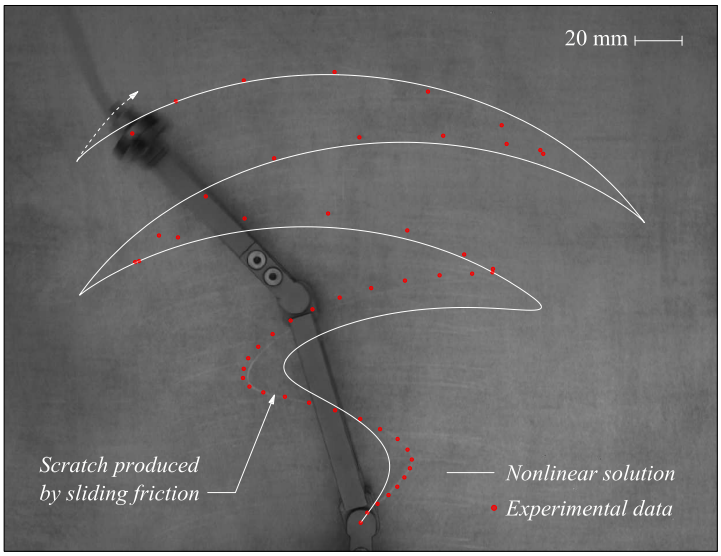

Fig. 7: The scratch left by the wheel on the plate compared with the nonlinear solution of Eqs. (7) with $W = (W_f + W_d)/2$, v_p =100 mm/s and initial conditions $\alpha_1 = \alpha_2 = 0^\circ$ and $\dot{\alpha}_1 = \dot{\alpha}_2 = 0.5\,\mathrm{rad/s}$. The red spots along the scratches are positions of the wheel corresponding to photos taken with the high speed camera; the scratch left during the experiment is clearly visible in the initial part of the test, not evidencing detachments. The whole sequence corresponds to 2.04 s.

aluminum plate during the experiments, using an optical microscope (with a Nikon SMZ800 stereo-zoom microscope equipped with Nikon Plan Apo 0.5x objective and a Nikon DD-FI1 high definition color camera head), without finding traces of detachments.

3 Experimental results

We have performed experiments with three different prototypes of the two-degree-of-freedom structure sketched in Figs. 3 and 4, always finding flutter and divergence instabilities for appropriate loads. In

the first prototype the elastic hinges were realized with thin steel strips working under flexure, while for the other structures these have been realized as true hinges without (in the case of the second prototype) and with (in the case of the third prototype) ball bearings. In this way the viscous behaviour of the hinges in the three prototypes was markedly different. We have tried a series of different wheel/plate friction conditions, first using an aluminum wheel sliding on paper, then sliding on P2000-sand paper, later, using a steel wheel sliding on a sandblasted-steel plate and, finally, we have used a steel wheel sliding against an aluminum plate. Since the rotational inertia of the wheel introduces a force transversal to the axis of the structure, we have checked the influence of this effect in the three prototypes by employing five different wheels, one in aluminum (V-shaped cross section, external diameter 15 mm, thickness 5 mm and weight 3 gr) and four in steel (one with V-shaped cross section, external diameter 25 mm, thickness 6 mm and weight 17 gr; three cylindrical with external diameter 25 mm, thicknesses 5, 6 and 10 mm and weights 18, 22 and 36 gr), so that we have proved that, within the dimension range of our prototypes, the mass of the wheel and the real dimensions of the contact area (which reduces to a point only in ideal conditions) do not affect much the instability.

The two initial prototypes have both broken during experiments to detect divergence instability, so that we have limited in the third prototype the stroke of the model. Precise measurements have been carried out only using the third prototype, specially designed with this purpose. While we will limit the presentation to the third prototype in the following, we stress now the point that since flutter was always observed at sufficiently high loading, the phenomenon has been found to occur: (i.) with the different viscosity related to the different mechanical realization of the hinges, (ii.) with different mass and shape of the wheel (iii.) with different contact and friction conditions at the wheel/plate contact (aluminum/paper, aluminum/P2000-sand paper, steel/sandblasted-steel, steel/aluminium) and (iv.) with different geometries and stiffnesses. In all cases, we have verified agreement with the theoretical modelling.

3.1 Experimental setting

The two-degree-of-freedom system sketched in Figs. 3 and 4 has been realized as shown in Fig. 8 with two 100 mm long stainless steel AISI 304 rods with a rectangular cross section of external dimensions equal to 30 mm $\times$ 10 mm. The rods are connected through hinges realized using ball bearings (SKF, model 628/5-2Z), with a torsional spring obtained from a (1 mm diameter) music wire ASTM A228. The wheel, of diameter d=25 mm, mounted (with two ball bearings SKF, model 618/5) at the top of the final rod is made of stainless steel AISI 304 and the structure is hinged (with two ball bearings SKF, model 61800) to the loading frame through a load cell (Gefran S.p.A., model OC-K5U-C3), to measure the axial force (along $\mathbf{e}_1$).

The plate sliding against the structure is a 500 mm$\times$1000 mm$\times$5 mm aluminium alloy 6082 plate moved through a linear drive unit (Damo S.r.l., model AMV120LB), equipped with an ABB servo motor (model BSM0400CN00) and controlled with and ABB servo drive (model BSD0400), both purchased from ABB Sace S.p.A. The plate has been polished with sandpaper P100. An IEPE accelerometer (PCB Piezotronics Inc., model 333B50) has been attached at the top of the final piece of the structure. Photos of the system have been taken with a high speed camera (Genie HM1400 from DALSA Corporation), equipped with AF Nikkor (18-35 mm 1:3.5-4.5 D) lens (Nikon Corporation) and a movie has been recorded during the whole test with a Sony handycam (model HDR-XR550VE). The axial force, the transversal acceleration (along $\mathbf{e}_\theta$) and the position of the plate have been acquired with a sample rate of 5 kS/s through a NI PXI-6221 data acquisition system, interfaced with Labview 8.5.1 (National Instruments).

The viscosity of the hinges has been measured in the following way. The central hinge of the system has been blocked, so that the structure has been reduced to a one-degree-of-freedom elastic

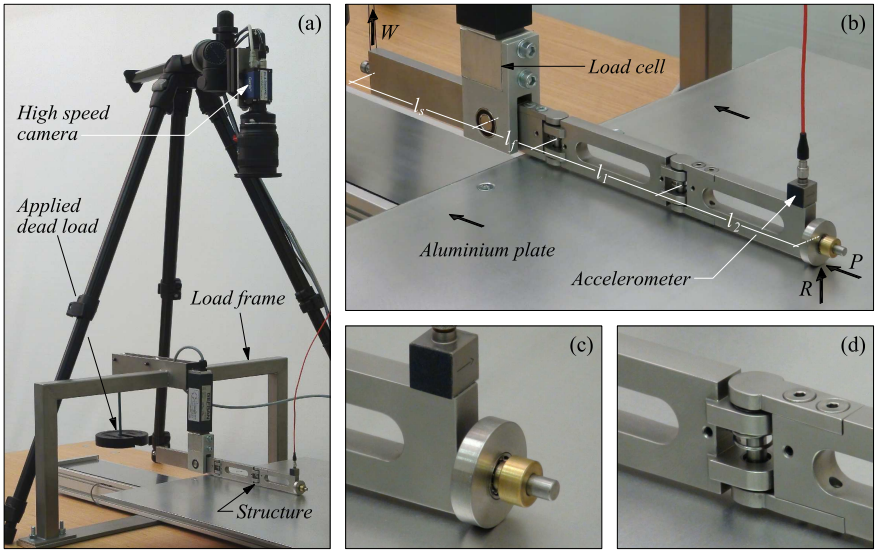

Fig. 8: The practical realization of the concept exemplified in Figs. 3 and 4. (a) A global view of the experimental setting; (b) a detail of the whole structure suffering instability; (c) detail of the structure: the wheel (a 25 mm diameter steel cylinder, 6 mm thick) and the accelerometer; (d) detail of the structure: an elastic hinge.

pendulum ($\alpha_1 = \alpha_2$), which has been left free of oscillating starting from an initial configuration at $\alpha_1 = 45°$, for different values of load W, with the plate advancing at a constant speed of 50 mm/s. The deformations of the structure have been recorded with the high-speed camera at 25 frames per second and the parameter β_1 has been estimated through comparison with the solution of the free damped vibrations of a pendulum. The results are reported in Tab. 1.

W_i	19.5 N	24.5 N	29.5 N	34.5 N	39.5 N
β_i	0.0036 N m s	0.0041 N m s	0.0052 N m s	0.0074 N m s	0.0095 N m s
Mean and standard deviation of the parameters β_1 and β_2= {0.006; 0.0025}N m s					

Tab. 1: Measured values of the viscosity parameters β_1 and β_2 as a function of the applied dead load W characterizing the structure shown in Fig. 8.

Although we have found that the viscosity of the hinges depends on W, an effect related to the fact that an increase in the applied weight yields an increase of the dissipation within the bearings, a good approximation (intended as the best 'compromise' with the factors that we have neglected) to the viscosity of the hinges (β_1 and β_2, taken to be equal), has been found that reported in Tab. 2, where all parameters characterizing the geometry and the mechanical behaviour of the structure shown in Fig. 8 have been reported, to be used for numerical simulations. The friction coefficients (between steel and

Lengths of the rods		Hinges charact.		General data	
l_1	100 mm	k_1	0.189 N m	ρ	1.84 g/mm
l_2	100 mm	k_2	0.189 N m	μ_s	0.61 ± 0.06
l_f	50 mm	β_1	0.006 N m s	μ_d	0.47 ± 0.05
l_s	125 mm	β_2	0.006 N m s	d	25 mm

Tab. 2: Measured valued of the parameters characterizing the structure shown in Fig. 8 and used in the numerical simulations.

aluminum) in the table have been evaluated from the mean values of the axial forces measured during

all the tests. The values of the friction coefficients have been found to be independent of the applied load W and to fit the values available in the literature (Minshall, 1992). Using the values listed in the table, we can estimate the critical loads for flutter and divergence from Eqs. (12). These, in the absence of viscosity ($\beta_1 = \beta_2 = 0$), result to be $W_f = 20.5\,\mathrm{N}$ and $W_d = 37.5\,\mathrm{N}$, which become 14.4 N and 55.9 N when the viscosity of the hinges is kept into account.

Note that all the values listed in Tab. 2 have been determined *independently* from flutter and divergence experiments and will be found to nicely fit these experiments.

3.2 The evidence of flutter and divergence instabilities induced by friction

Since the interval of load W corresponding to flutter and divergence is known, we can test these instabilities on the structure shown in Fig. 8 (b) by increasing the load W from a stable situation. The result is shown in Fig. 9, where an experimental investigation of the critical loads for flutter and divergence instability is reported. We have not found any dependence of the critical loads on the plate velocity v_p, which has been imposed equal to 50 mm/s to measure the values reported in Fig. 9. Note that the elastic model predicts flutter at W_f and divergence at W_d and this interval

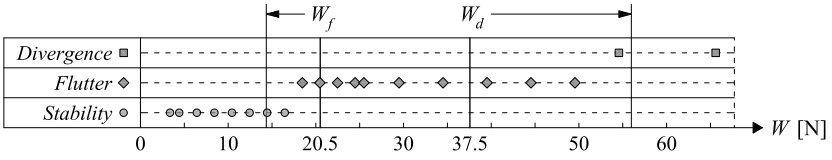

Fig. 9: Experimental investigation on flutter and divergence instability at increasing load W at v_p=50 mm/s. The elastic model predicts flutter instability to occur at W_f and divergence at W_d; these values are corrected to $0.70\,W_f$ and $1.49\,W_d$ when viscosity at the hinges is included.

is 'broadened' (note the arrows in the figure) to $0.7\,W_f$ and $1.49\,W_d$, when viscosity of the hinges is kept into account (see Appendix A). This broadening of the flutter range is consistent with our experimental results shown in Fig. 9. The discrimination between stability and flutter instability has been performed through visual inspection and documented with the photographic record. This discrimination has been found easy, while some difficulties have been encountered in distinguishing between flutter and divergence instability in the transition zone between the two phenomena.

A sequence of photos taken with the high-speed camera (with the Sony handycam) at 25 shots per second is shown in Fig. 10 (in Fig. 11) documenting a case of *flutter instability* at a load $W = (W_f + W_d)/2 = 29\,\mathrm{N}$ and a speed of 75 mm/s of the aluminum plate.

The vibrational motion of increasing amplitude is evident from both Figs. 10 and 11. The same test is also documented in a movie provided in the electronic supplementary material (see also http://ssmg.ing.unitn.it/). Note that the sequence of photos corresponds to the sequence of configurations reported in Fig. 6 (upper part), so that the direct comparison results to be excellent.

The measured acceleration versus time during a flutter test at a load $W = (W_f + W_d)/2 = 29\,\mathrm{N}$ are reported in Fig. 12, for a plate velocity of 75 mm/s (a detail of the curve on the left is shown on the right). Results of the numerical nonlinear (linear viscoelastic) simulation are also reported in red (in blue) for the initial 6 s (1.5 s), with initial conditions $\alpha_1 = \alpha_2 = 0.5°$ and $\dot{\alpha}_1 = \dot{\alpha}_2 = 0$. Note from Fig. 12 the initial increase in the amplitude of the acceleration, denoting flutter, and the following stabilization, when a steady situation is reached. *The attainment of a steady dynamics at large displacement is an important conclusion of our study.*

It is important to point out that, although the onset of flutter and the transition between flutter

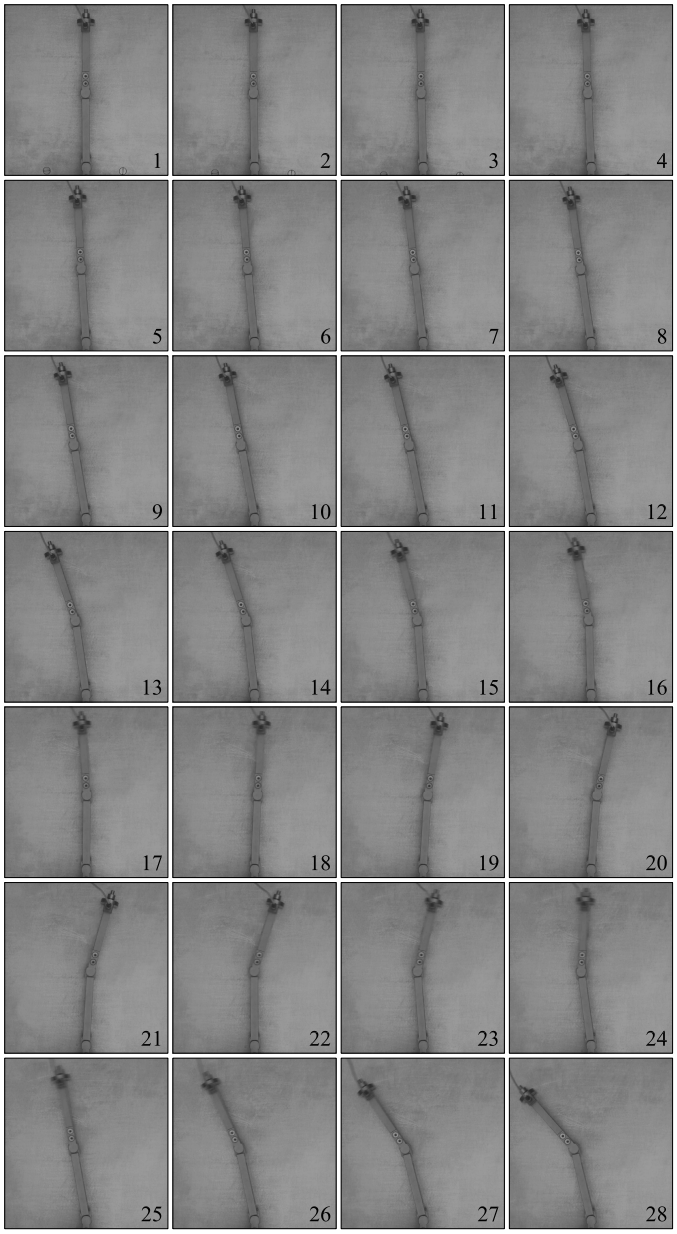

Fig. 10: A sequence of photos (taken with a high-speed camera at 25 frames per second) of the structure sketched in the lower part of Fig. 8 and exhibiting flutter instability. Note the blurred photos, denoting increasing velocity of the motion. The whole sequence of photos has been recorded in 1.08 seconds and the time interval between two photos was 0.04 seconds. The experiment refers to $W = (W_f + W_d)/2$ and $v_p = 75\,\mathrm{mm/s}$. The plate is advancing vertically from the top to the bottom. This sequence of photos can directly be compared with the sequence of configurations shown in Fig. 6, upper part.

and divergence have been found independent of the plate velocity, we have found a dependence on this velocity of the *maximum amplitude of displacement reached during steady motion in flutter conditions*. This dependence is connected with the attainment of the stick/slip condition $\dot{C}_p^r \leq \varepsilon$, in the sense that the smaller is the velocity, the earlier the stick condition is attained and the oscillation inverted. This behaviour is consistent with the fact that the velocity of the plate is essential to satisfy the sliding

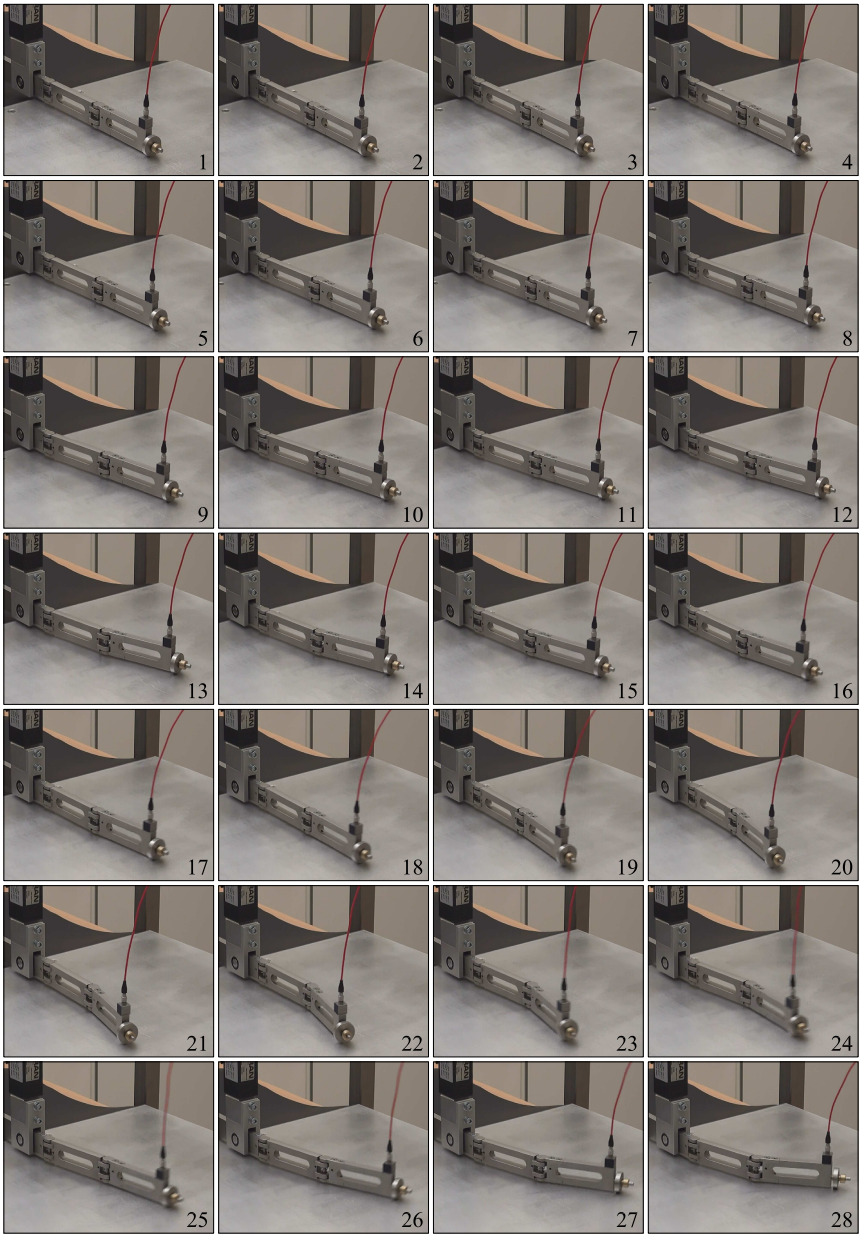

Fig. 11: A sequence of photos (taken from a movie recorded with a Sony handycam at 25 frames per second) of the structure sketched in the lower part of Fig. 8 and exhibiting flutter instability. The whole sequence of photos has been recorded in 1.08 seconds and the time interval between two photos was 0.04 seconds. The experiment refers to $W = (W_f + W_d)/2$ and $v_p = 75\,\mathrm{mm/s}$.

condition and ensures the validity of the linearized analysis to capture the onset of the instability. It is clear that the effects of the instability become more 'intense' when the velocity of the plate is increased. These observations are fully confirmed by the numerical simulations of the nonlinear equations (7), so that a comparison between theoretical predictions and measured values is reported in Fig. 13.

Two sequences of photos taken with the high-speed camera and with the Sony handycam, both at 25 shots per second, is shown in Fig. 14, documenting a case of *divergence instability* at a load

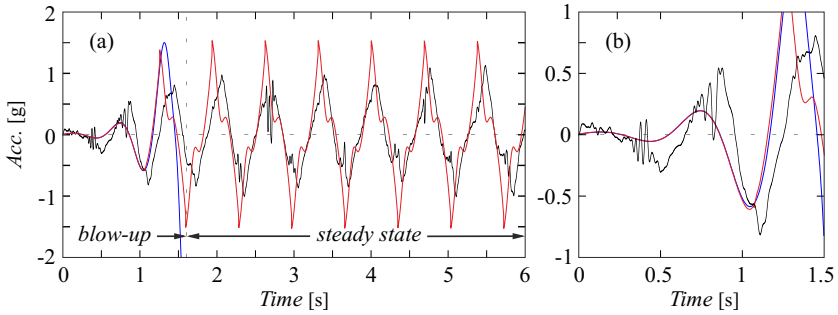

Fig. 12: Measured acceleration versus time (6 seconds are reported) during the flutter test reported in Figs. 10 and 11, at a load $W = (W_f + W_d)/2$ and for a plate velocity of 75 mm/s. The part on the right is a detail of the part on the left, referred to the initial 1.5 s. Results of the numerical nonlinear (linear with viscosity) simulation at the same load and with initial conditions $\alpha_1 = \alpha_2 = 0.5°$ are reported in red (in blue). The solution of the linear equations (blue curve) has been interrupted at 1.5 s since the blow-up was too high. Note the initial increase in the amplitude of the acceleration denoting flutter (well captured even by the linearized viscoelastic analysis), and the following stabilization (captured by the nonlinear analysis), due to the effect of the nonlinearities.

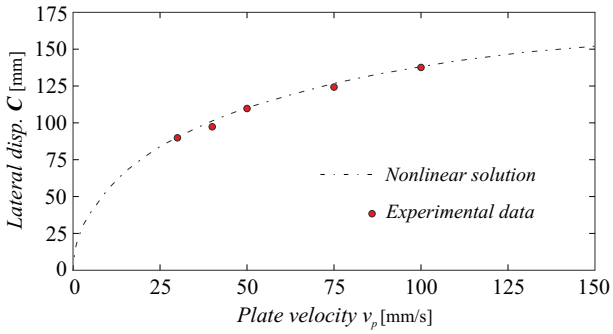

Fig. 13: Maximum lateral displacement of the end point **C** of the structure as a function of the plate velocity v_p when the steady state motion is reached. The dashed curve is obtained through the numerical solution of Eqs. (7), for different plate velocities and an applied dead load $W = (W_f + W_d)/2$; the red spots are the experimental data.

$1.75\,W_d$ and a speed of 50 mm/s of the aluminum plate. In the experimental setting a lateral rubber constraint has been added to prevent possible failure of the equipment. In fact the motion caused by divergence instability has been found to be particularly violent. The exponential growth of displacement connected to the divergence instability is clearly visible in the figure. Note that the sequence of photos can be directly compared with the sequence of configurations shown in Fig. 6, lower part, and shows an excellent agreement.

Finally, a case of stability is documented with a 5 seconds long sequence of photos, taken (with a Sony handycam) at a time intervals of 1 s, and is reported in Fig. 15 at a load W=5 N, and at a speed of the aluminum plate of 50 mm/s.

During our experiments we have also recorded the noise generated during sliding and we have carefully observed the rotational motion of the wheel. The emitted noise highlights the vibrational character of flutter instability and the rotational motion of the wheel shows that there is no inversion of the rotation before the end of an oscillation is reached, in agreement with our model.

In closure, we note that all instabilities are suppressed in our system if the central hinge (Fig. 8 d) is blocked, since the follower load induced by friction does not work. Moreover, divergence instability and buckling occur, *but not flutter*, if the wheel is prevented from rotating. These two behaviours

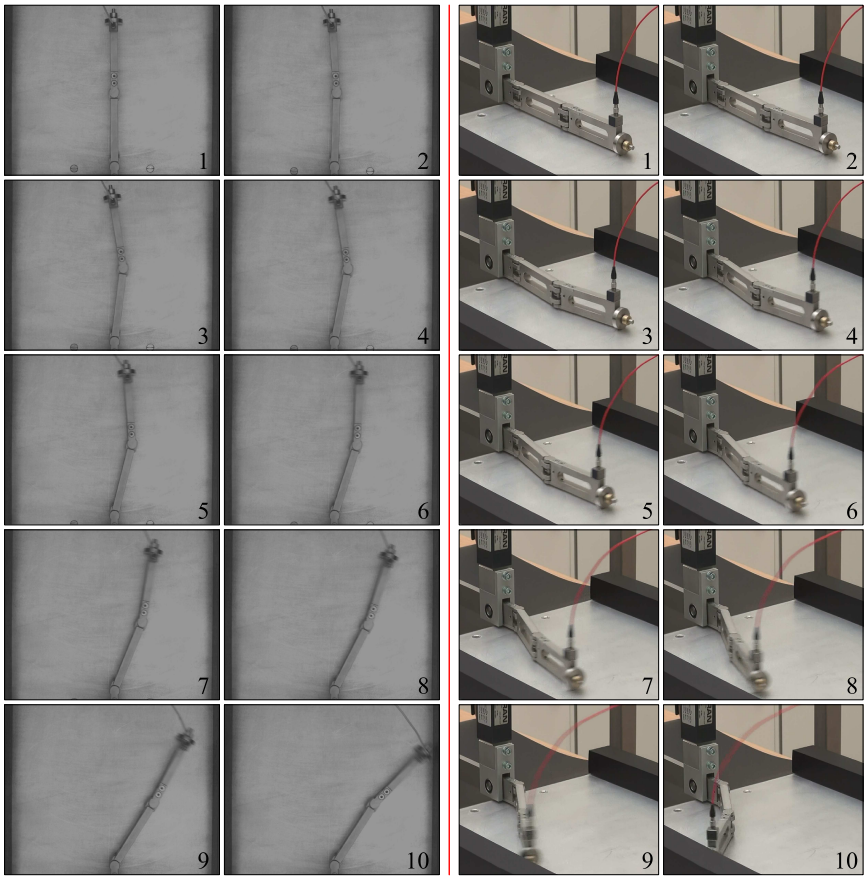

Fig. 14: Two sequences of photos (taken with a high-speed camera, on the left, and with a Sony handycam, on the right, at 25 frames per second) of the structure sketched in the lower part of Fig. 8 and exhibiting divergence instability. Note the blurred photos, denoting increasing velocity of the motion. The whole sequence of photos has been recorded in 0.36 seconds and the time interval between two photos was 0.04 seconds. The experiment refers to $W = 1.75\, W_d$ and $v_p = 50\,\text{mm/s}$. The sequence of photos on the left can be directly compared with the sequence of configurations shown in Fig. 6, lower part.

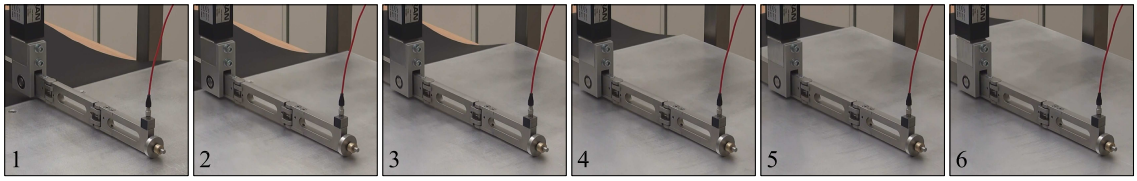

Fig. 15: A sequence of photos (taken with a Sony handycam) of the structure sketched in the lower part of Fig. 8 within the region of stability. The whole sequence of photos has been recorded in 5 s and the time interval between two photos was 1 s. The experiment refers to W=5 N and $v_p = 50\,\text{mm/s}$.

have been both studied and checked experimentally, see Appendix B.

4 A final discussion

Flutter and divergence instabilities have been experimentally demonstrated to occur in a two-degree-of-freedom elastic structure, as related to dry friction, in full agreement with theoretical predictions. In particular, all the following phenomena, documented in various experiments with different settings, are all quantitatively predicted by the theoretical modelling and fully interpretable as friction-induced flutter or divergence instabilities.

- Experiments performed on three different realizations of the structure sketched in Figs. 3 and 4 have all shown at increasing load: nearly-null vibrations (interpreted as stable behaviour, Fig. 15), blowing-up oscillations becoming large and steady after 1–2 seconds (interpreted as flutter, Figs. 10 and 11) and, finally, exponentially growing motion (interpreted as divergence instability, Fig. 14).

- Since the three structures had different geometries, stiffnesses, types of elastic hinges and wheel/plate friction coefficients, the instabilities are quantitatively *but not qualitatively* affected by all these parameters and, in particular, by the viscosity at articulations and by the value of the friction coefficient at the wheel/plate contact.

- While the amplitude of the vibrations during steady motion has been found to depend on the sliding velocity of the plate, the onset of flutter has been found independent of this.

- The *accelerations* measured at the tip of the structure and the *noise* recorded during the tests show initially an oscillatory blow-up, which finally reaches a steady-state, during flutter instability (Fig. 12).

- No evidences of detachment at the wheel/plate contact have been found at a microscope investigation of the scratches on the plate.

- The wheel rotates during instability and does not invert rotation before the end of an oscillation.

- When the wheel is prevented from rotating, three behaviours are found at increasing load: nearly-null vibrations (interpreted as stable behaviour), growing motion with low acceleration and without vibrations (interpreted as divergence instability, Fig. 17 upper part) and, finally, stick of the wheel with flexure of the structure (interpreted as buckling, Fig. 17 lower part).

- When the central hinge of the structure is blocked, the structure is found to have nearly-null vibrations at every load level (stable behaviour, Fig. 18).

Neither any evidence against the model of flutter or divergence instabilities, nor possibilities of describing these phenomena with different models, have been found. Our experiments show that a follower load of tangential type can be easily obtained by exploiting a constraint with Coulomb friction. Moreover, the fully nonlinear dynamics which develops in flutter conditions shows that the system reaches a steady state, in which the maximum amplitude of the motion depends on the initial relative velocity at the friction contact.

Acknowledgments

The authors gratefully acknowledge financial support from the University of Trento.

Appendix A Details of the analysis for the two d.o.f. system shown in Fig. 1

We provide details of the stability analysis of the structure shown in Fig. 1, which have been omitted in Section 2.

Denoting the time derivative by a superimposed dot, the velocities of points $\mathbf{C}$, $\mathbf{G}_1$ and $\mathbf{G}_2$ can be obtained from Eqs. (1) as

$$\begin{aligned}
\dot{\mathbf{C}} &= -(l_1\dot{\alpha}_1 \sin\alpha_1 + l_2\dot{\alpha}_2 \sin\alpha_2)\mathbf{e}_1 + (l_1\dot{\alpha}_1 \cos\alpha_1 + l_2\dot{\alpha}_2 \cos\alpha_2)\mathbf{e}_2, \\
\dot{\mathbf{G}}_1 &= -[(l_1/2)\dot{\alpha}_1 \sin\alpha_1]\mathbf{e}_1 + [(l_1/2)\dot{\alpha}_1 \cos\alpha_1]\mathbf{e}_2, \\
\dot{\mathbf{G}}_2 &= -[l_1\dot{\alpha}_1 \sin\alpha_1 + (l_2/2)\dot{\alpha}_2 \sin\alpha_2]\mathbf{e}_1 + [l_1\dot{\alpha}_1 \cos\alpha_1 + (l_2/2)\dot{\alpha}_2 \cos\alpha_2]\mathbf{e}_2,
\end{aligned} \tag{A.1}$$

so that the accelerations of the mass center of the two rigid bars are

$$\begin{aligned}
\ddot{\mathbf{G}}_1 &= -[(l_1/2)(\ddot{\alpha}_1 \sin\alpha_1 + \dot{\alpha}_1^2 \cos\alpha_1)]\mathbf{e}_1 + [(l_1/2)(\ddot{\alpha}_1 \cos\alpha_1 - \dot{\alpha}_1^2 \sin\alpha_1)]\mathbf{e}_2, \\
\ddot{\mathbf{G}}_2 &= -[l_1(\ddot{\alpha}_1 \sin\alpha_1 + \dot{\alpha}_1^2 \cos\alpha_1) + (l_2/2)(\ddot{\alpha}_2 \sin\alpha_2 + \dot{\alpha}_2^2 \cos\alpha_2)]\mathbf{e}_1 + \\
&\quad +[l_1(\ddot{\alpha}_1 \cos\alpha_1 - \dot{\alpha}_1^2 \sin\alpha_1) + (l_2/2)(\ddot{\alpha}_2 \cos\alpha_2 - \dot{\alpha}_2^2 \sin\alpha_2)]\mathbf{e}_2.
\end{aligned} \tag{A.2}$$

The expressions (A.1) and (A.2) are employed to write down the principle of virtual works (6), from which the differential equations governing the dynamics of the structure, Eqs. (7), follow.

A.1 Linearized analysis of the elastic structure

For a flutter analysis in the absence of viscosity, solutions of the linearized equations of motion (10) are sought in the time-harmonic form

$$\alpha_j = A_j\, e^{-i\Omega t}, \quad j = 1, 2 \tag{A.3}$$

where A_j are (complex) amplitudes, Ω is the circular frequency, and i is the imaginary unit ($i = \sqrt{-1}$), so that a substitution of Eq. (A.3) into Eqs. (10) yields

$$\begin{bmatrix} (1+\lambda/3)\omega^2 + \gamma - k - 1 & \omega^2/(2\lambda) - \gamma + 1 \\ \omega^2/(2\lambda) + 1 & \omega^2/(3\lambda^2) - 1 \end{bmatrix} \begin{Bmatrix} A_1 \\ A_2 \end{Bmatrix} = \begin{Bmatrix} 0 \\ 0 \end{Bmatrix}, \tag{A.4}$$

where

$$\gamma = \frac{Pl_1}{k_2}, \qquad \omega^2 = \frac{l_1^2 l_2 \rho}{k_2}\Omega^2. \tag{A.5}$$

Non-trivial solution of system (A.4) is possible if the determinant of the matrix vanishes, a condition which immediately provides the solutions

$$\omega^2 = \frac{b(\gamma) \pm \sqrt{\Delta(\gamma)}}{1 + (4/3)\lambda}, \tag{A.6}$$

where

$$\Delta(\gamma) = b^2(\gamma) - 4k\lambda^2(3 + 4\lambda) \quad \text{and} \quad b(\gamma) = -\gamma(2 + 3\lambda) + 2(1 + \lambda)^3 + 2k, \tag{A.7}$$

so that

$$\Omega = \frac{1}{l_1}\sqrt{\frac{k_2}{l_2\rho}}\,\omega. \tag{A.8}$$

We note that $k > 0$, $\lambda > 0$, $\Delta(\gamma) < b^2(\gamma)$ and that

$$\begin{aligned} b(\gamma) > 0 \quad &\Leftrightarrow \quad \gamma < \frac{k + (1+\lambda)^3}{1 + (3/2)\lambda}, \\ \Delta(\gamma) < 0 \quad &\Leftrightarrow \quad 0 < \frac{k + (1+\lambda)^3 - \lambda\sqrt{k(3+4\lambda)}}{1 + (3/2)\lambda} < \gamma < \frac{k + (1+\lambda)^3 + \lambda\sqrt{k(3+4\lambda)}}{1 + (3/2)\lambda}, \end{aligned} \tag{A.9}$$

so that following three possibilities only arise:

- two real and positive values for ω^2, corresponding to $b(\gamma) > 0$ and $\Delta(\gamma) > 0$. There are four Ω, two positive and two negative and vibrations are sinusoidal, a situation which corresponds to *stability*;
- two complex conjugate values for ω^2, corresponding to $\Delta(\gamma) < 0$. There are two complex-conjugate pairs of Ω, so that there are four exponential solutions, two blowing up and the other two decaying with time, a situation corresponding to *flutter instability*;
- two real and negative values for ω^2, corresponding to $b(\gamma) < 0$ and $\Delta(\gamma) > 0$. There are two purely imaginary complex-conjugate pairs of Ω, so that vibrations are exponential with time (one amplifying and the other decaying), a situation corresponding to *divergence instability*.

As a conclusion

- *flutter instability* occurs when $\gamma_f < \gamma < \gamma_d$, where

$$\underset{d}{\gamma_f} = \frac{k + (1+\lambda)^3 \mp \lambda\sqrt{k(3+4\lambda)}}{1 + (3/2)\lambda}, \tag{A.10}$$

  which is identical (though written in a different notation) to Eq. (12),
- and *divergence instability* occurs when $\gamma > \gamma_d$.

A.2 Linearized analysis of the viscoelastic structure

A linear viscoelastic analysis can be performed through a linearization of Eqs. (7) near the trivial solution ($\alpha_1 = \alpha_2 = 0$), yielding

$$\begin{cases} \dfrac{1}{3}\rho l_1^2 (l_1 + 3l_2)\,\ddot{\alpha}_1 + \dfrac{1}{2}\rho l_1 l_2^2 \ddot{\alpha}_2 + (\beta_1 + \beta_2)\dot{\alpha}_1 - \beta_2\dot{\alpha}_2 + (k_1 + k_2)\alpha_1 + \\ -k_2\alpha_2 - l_1 P(\alpha_1 - \alpha_2) = 0, \\ \dfrac{1}{2}\rho l_1 l_2^2 \ddot{\alpha}_1 + \dfrac{1}{3}\rho l_2^3 \ddot{\alpha}_2 - \beta_2(\dot{\alpha}_1 - \dot{\alpha}_2) - k_2(\alpha_1 - \alpha_2) = 0. \end{cases} \tag{A.11}$$

Looking for time-harmonic vibrations near the equilibrium configuration, we seek solutions of Eqs. (A.11) in the form (A.3), so that a substitution into Eqs. (A.11) yields

$$\begin{bmatrix} (1+\lambda/3)\omega^2 + \eta(\beta+1)\omega - \gamma + k + 1 & \omega^2/(2\lambda) - \omega\eta + \gamma - 1 \\ \omega^2/(2\lambda) - \omega\eta - 1 & \omega^2/(3\lambda^2) + \omega\eta + 1 \end{bmatrix} \begin{Bmatrix} A_1 \\ A_2 \end{Bmatrix} = \begin{Bmatrix} 0 \\ 0 \end{Bmatrix}, \tag{A.12}$$

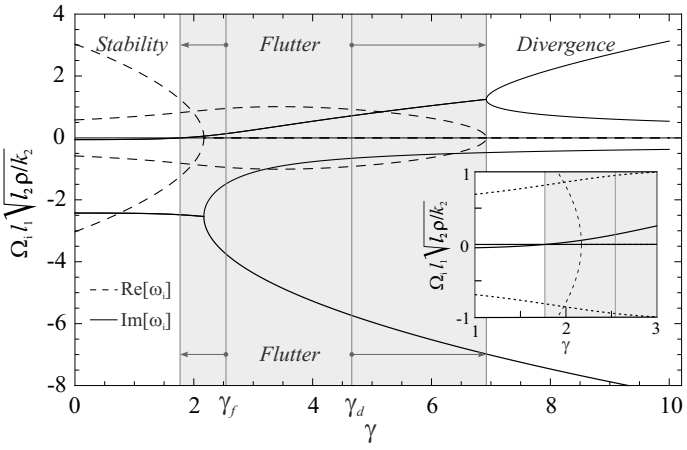

Fig. 16: Real and imaginary part of the solutions $\Omega_i\, l_1\sqrt{l_2\rho/k_2}$ as a function of the loading parameter γ and obtained solving the characteristic equation (A.14). Note the broadening of the flutter region due to damping.

where

$$\beta = \frac{\beta_1}{\beta_2}, \qquad \omega = -i\, l_1\sqrt{\frac{l_2\rho}{k_2}}\,\Omega, \qquad \eta = \sqrt{\frac{\beta_2^2}{l_1^2 l_2 k_2 \rho}}. \tag{A.13}$$

Non-trivial solution of system (A.12) is possible if the determinant of the matrix vanishes, a condition which immediately provides the characteristic equation

$$p_0\omega^4 + p_1\omega^3 + p_2\omega^2 + p_3\omega + p_4 = 0, \tag{A.14}$$

where the coefficients are

$$\begin{aligned} p_0 &= 1/4 + \lambda/3 > 0, \\ p_1 &= \eta[\beta + (1+\lambda)^3] > 0, \\ p_2 &= \lambda^3 + 3\lambda^2(1+\beta\eta^2) + 3\lambda + k - \gamma(1 - 3\lambda/2) + 1, \\ p_3 &= 3\lambda^2(k+\beta)\eta > 0, \\ p_4 &= 3\lambda^2 k > 0. \end{aligned} \tag{A.15}$$

In this context, we have the following possibilities for a solution Ω_i:

- $\mathrm{Im}[\Omega_i] < 0$ stability,
- $\mathrm{Im}[\Omega_i] > 0$ and $\mathrm{Re}[\Omega_i] \neq 0$ flutter,
- $\mathrm{Im}[\Omega_i] > 0$ and $\mathrm{Re}[\Omega_i] = 0$ divergence.

The numerical determination of the solutions of Eq. (A.14), assuming $\lambda = k = \beta = 1$ and $\eta = 0.32$, the values corresponding to the structure tested in our experiments (Tab. 2), reveals that flutter occurs within the interval $0.70W_f < W < 1.49W_d$, while for $W < 0.70W_f$ the system is stable and, finally, divergence occurs for $W > 1.49W_d$. The situation is sketched in Fig. 16, where the real and imaginary parts of the solutions $\Omega_i\, l_1\sqrt{l_2\rho/k_2}$ are reported as a function of the loading parameter γ. In the figure, the values γ_f and γ_d correspond to flutter and divergence instabilities in the absence of viscosity, so that we may see that the introduction of the viscosity broadens the interval of flutter.

Appendix B Wheel prevented from rotating and one-degree-of-freedom system

To complete our study, we analyze the case in which the wheel in the structure shown in Fig. 8(c) is blocked and the case in which the structure is reduced to a one-degree-of-freedom system by blocking the central hinge (but leaving free the wheel). In the former case there is no flutter, but divergence and buckling occur, whereas in the latter case the behaviour is always stable. Our experiments confirm these theoretical findings.

B.1 Wheel prevented from rotating

If the wheel is replaced with a fixed contact (we have blocked the wheel with a screw), the system becomes subjected to a frictional force, which assuming sliding can be written as

$$\mathbf{P} = -P\,\frac{\dot{\mathbf{C}}_p}{|\dot{C}_p|}, \qquad P = \mu_d\,\frac{l_s}{l_f + l_1\cos\alpha_1 + l_2\cos\alpha_2}\,W. \tag{B.1}$$

Eq. (B.1), can be linearized near the configuration $\alpha_1 = \alpha_2 = 0$ assuming $v_p >> l_1\dot{\alpha}_1 + l_2\dot{\alpha}_2$, so that it becomes

$$\mathbf{P} = -\{P\}\mathbf{e}_1 - \{P(l_1\dot{\alpha}_1 + l_2\dot{\alpha}_2)/v_p\}\mathbf{e}_2, \qquad P = \mu_d\,\frac{l_s}{l_f + l_1 + l_2}\,W, \tag{B.2}$$

and Eqs. (10) become

$$\begin{cases} \dfrac{1}{3}\rho l_1^2\,(l_1 + 3l_2)\,\ddot{\alpha}_1 + \dfrac{1}{2}\rho l_1 l_2^2\ddot{\alpha}_2 + (k_1 + k_2)\alpha_1 - k_2\alpha_2 - l_1 P\alpha_1 + l_1 P\,\dfrac{l_1\dot{\alpha}_1 + l_2\dot{\alpha}_2}{v_p} = 0, \\ \dfrac{1}{2}\rho l_1 l_2^2\ddot{\alpha}_1 + \dfrac{1}{3}\rho l_2^3\ddot{\alpha}_2 - k_2\alpha_1 + k_2\alpha_2 - l_2 P\alpha_2 + l_2 P\,\dfrac{l_1\dot{\alpha}_1 + l_2\dot{\alpha}_2}{v_p} = 0. \end{cases} \tag{B.3}$$

We look now for time-harmonic vibrations near the equilibrium configuration, so that the Lagrangean parameters are now assumed to be harmonic functions of time, Eq. (A.3), so that a substitution into Eqs. (B.3) yields

$$\begin{bmatrix} (1+\lambda/3)\omega^2 + \gamma\nu\omega - \gamma + k + 1 & \omega^2/(2\lambda) + \omega\gamma\nu/\lambda - 1 \\ \omega^2/(2\lambda) + \omega\gamma\nu/\lambda - 1 & \omega^2/(3\lambda^2) + \omega\gamma\nu/\lambda^2 - \gamma/\lambda + 1 \end{bmatrix} \begin{Bmatrix} A_1 \\ A_2 \end{Bmatrix} = \begin{Bmatrix} 0 \\ 0 \end{Bmatrix}, \tag{B.4}$$

where

$$\omega = -i\,l_1\sqrt{\frac{l_2\rho}{k_2}}\,\Omega, \qquad \nu = \frac{1}{v_p}\sqrt{\frac{k_2}{l_2\rho}}. \tag{B.5}$$

Non-trivial solution of system (B.4) is possible if the determinant of the matrix vanishes, a condition which provides the characteristic equation

$$p_0\omega^4 + p_1\omega^3 + p_2\omega^2 + p_3\omega + p_4 = 0, \tag{B.6}$$

where the coefficients are

$$\begin{aligned} p_0 &= 1/4 + \lambda/3, \\ p_1 &= \gamma(1+\lambda)\nu, \\ p_2 &= k + (1+\lambda)^3 - \gamma[1 + \lambda(3+\lambda)], \\ p_3 &= 3\gamma[k + (1 - \gamma + \lambda)(1+\lambda)]\nu, \\ p_4 &= 3\lambda[\gamma^2 + k\lambda - \gamma(1 + k + \lambda)]. \end{aligned} \tag{B.7}$$

The stability of the system can be analyzed using the Routh–Hurwitz criterion (Ziegler, 1977), which ensures that all the ω_i have negative real part; the criterion for stability requires that

$$\begin{aligned} p_1 &> 0, \\ p_1 p_2 - p_0 p_3 &> 0, \\ (p_1 p_2 - p_0 p_3) p_3 - p_1^2 p_4 &> 0, \\ p_4 &> 0. \end{aligned} \tag{B.8}$$

Conditions (B.8) are equivalent to

$$\gamma < \gamma_{cr} = \frac{1 + k + \lambda - \sqrt{(1+k)^2 + \lambda(2 - 2k + \lambda)}}{2}, \tag{B.9}$$

corresponding to the buckling load of the two degree-of-freedom structure, when subjected to a compressive dead load $-\{P\}\mathbf{e}_1$. For $\gamma > \gamma_{cr}$ the structure is unstable and in fact divergence has been experimentally detected, as shown by the example reported in Fig. 17, upper part, referred to a load $W = 6.5\,\mathrm{N}$. Regarding this instability, we note that its onset is difficult to be detected, since the

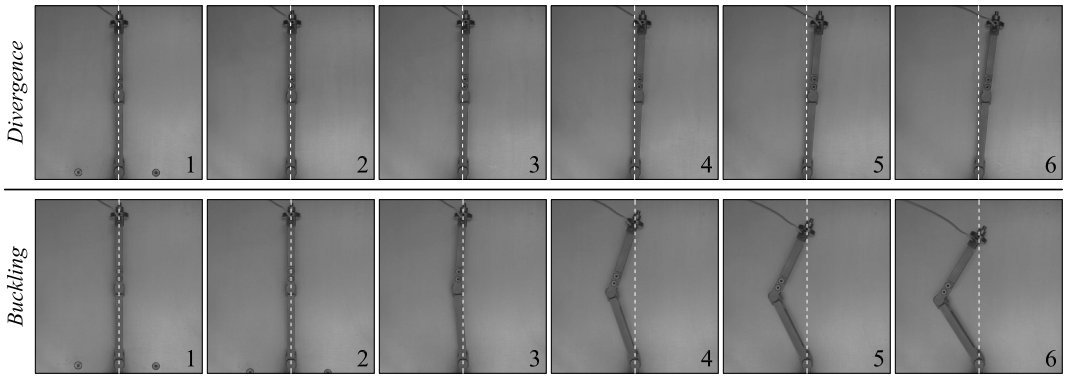

Fig. 17: The structure with fixed wheel exhibiting divergence (upper part) and buckling (lower part). The time interval between two consecutive deformed shapes is 1 s for divergence and 0.2 s for buckling, while the whole sequence corresponds to 5 seconds for divergence and to 1 second for buckling. The applied dead loads are, respectively, W=6.5 N and W=16.5 N, while the velocity of the plate is 50 mm/s in both cases.

instability has an extremely mild character and may manifest itself only after a long plate sliding. Therefore, although the Routh–Hurwitz criterion provides a stability limit of 3.1 N, since the stroke of our plate is only 1 m, we have been able to detect the instability only from a load of 6 N.

Another, more evident, instability has been observed in our experiments (see Fig. 17, lower part) at an applied load W higher than that predicted by the Routh–Hurwitz criterion. In this instability, the wheel already sticks before the plate begins to move, so that a progressive buckling occurs without involving any relative movement at the wheel/plate contact. In this case, the system is reduced to a single degree-of-freedom structure (lower part of Fig. 17) and the critical load can be easily calculated to be (we recall that $\gamma = Pl_1/k_2$)

$$\gamma_{cr}^b = \frac{k}{1+\lambda} + \lambda + 1, \tag{B.10}$$

which, assuming a value for static friction, corresponds to a force W that can be easily calculated. We have found a good agreement of the experiment shown in Fig. 17, lower part, which refers to an applied load equal to 16.5 N, with the calculated γ_{cr}^b, corresponding to a load W equal to 15.5 N.

Note that $\gamma_{cr}^{b} \geq \gamma_{cr}$, so that if the structure would be kept fixed and so 'forced' to reach the slip condition, the divergence dynamical instability would occur instead of the buckling, possibly involving stick and slip.

B.2 System reduced to one degree-of-freedom by blocking the central hinge

When the central hinge in the structure shown in Fig. 8 (d) is fixed and the wheel is left free of rotating, stability is always verified, since the follower force does not work. We have confirmed this behaviour with a series of experiments in which the central hinge has been fixed. In these experiments we have raised the vertical load W until 50 N (well inside the region of divergence for the 2 d.o.f. structure), without finding sensible oscillations. A sequence of photos taken during one of these experiments is reported in Fig. 18, where we observe that the structure remains straight.

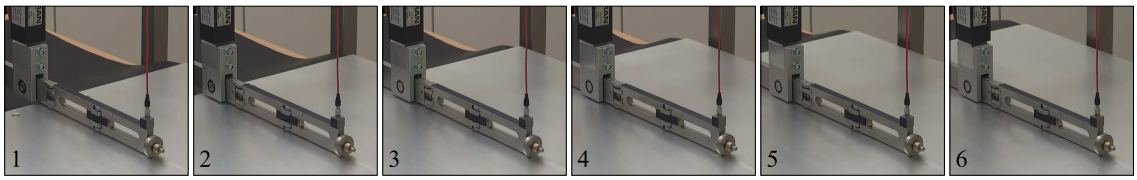

Fig. 18: A sequence of photos (taken with a Sony handycam) of the structure with a single d.o.f. (the hinge between the two rods has been fixed), demonstrating stability. The whole sequence of photos has been recorded in 5 seconds, so that the time interval between two photos is 1 seconds. The plate velocity was v_p=50 mm/s and the load W was equal to 29 N.

References

[1] Beck, M. (1952) Die Knicklast des einseitig eingespannten, tangential gedrückten Stabes. *Z. Angew. Math. Phys.*, 3, 225-228.

[2] Bigoni, D. (1995) On flutter instability in elastoplastic constitutive models. *Int. J. Solids Structures*, 32, 3167-3189.

[3] Bigoni, D. and Loret, B. (1999) Effects of elastic anisotropy on strain localization and flutter instability in plastic solids. *J. Mech. Phys. Solids*, 47, 1409-1436.

[4] Bigoni, D. and Petryk, H. (2002) A note on divergence and flutter instabilities in elastic-plastic materials. *Int. J. Solids Structures*, 39, 911-926.

[5] Bolotin, V.V. (1963) *Nonconservative problem of the theoty of elastic stability.* Pergamon Press, New York.

[6] Como, M. (1966) Lateral buckling of a cantilever subjected to a transverse follower force. *Int. J. Solids Structures*, 2, 515-523.

[7] Elishakoff, I. (2005) Controversy associated with the so-called "follower force": critical overview. *Appl. Mech. Rev.*, 58, 117-142.

[8] Flint, J. and Hultén, J. (2002) Lining-deformation-induced modal coupling as squeal generator in a distributed parameter disk brake model. *J. Sound and Vibration*, 254, 1-21.

[9] Herrmann, G. and Jong, I.C. (1965) On the destabilizing effect of damping in nonconservative elastic system. *J. Appl. Mech.*, 32, 592-597.

[10] Herrmann, G., Nemat-Nasser, S. and Prasad, S.N. (1966) Models demonstrating instability of nonconservative dynamical systems. Tech. Rept. No. 66-4, Northwestern University, Dept. of Civil Engineering.

[11] Herrmann, G. (1971) Dynamics and stability of mechanical systems with follower forces. Tech. Rept. NASA CR-1782.

[12] Koiter, W.T. (1996) Unrealistic follower forces. *J. Sound and Vibration*, 194, 636-638.

[13] Kröger, M., Neubauer, M. and Popp, K. (2008) Experimental investigation on the avoidance of self-excited vibrations. *Phil. Trans. R. Soc.*A 366, 785-810.

[14] Loret, B. (1992) Does deviation from deviatoric associativity lead to the onset of flutter instability? *J. Mech. Phys. Solids*, 40, 1363-1375.

[15] Loret, B., Simões, F.M.F. and Martins, J.A.C. (2000) Flutter instability and ill-posedness in solids and fluid-saturated porous media. In: Petryk, H. (Ed.), Material Instabilities in Elastic and Plastic Solids, CISM Lecture Notes No. 414, Springer-Verlag, Wien-New York, 109-207.

[16] Martins, J.A.C., Barbarin, S., Raous, M. and Pinto da Costa, A. (1999) Dynamic stability of finite dimensional linearly elastic systems with unilateral contact and Coulomb friction. *Comput. Meth. Appl. Mech. Engrg.*, 177, 289-328.

[17] Martins, J.A.C., Oden, J.T. and Simões, F.M.F. (1990) Recent advances in engineering science. A study of static and kinetic friction. *Int. J. Eng. Sci.*, 28, 29-92.

[18] Minshall, H. (1992) Coefficient of Friction Table. In: Lide, D.R. (Ed.), CRC Handbook of Chemistry and Physics, 73rd Edition. CRC Press, Boca Raton.

[19] Nguyen, Q.S. (1995) *Stabilité des structures élastiques*. Springer-Verlag.

[20] Nguyen, Q.S. (2003) Instability and friction. *Comptes Rendus Mécanique*, 331, 99-112.

[21] Nikolai, E.L. (1928) On the stability of the rectilinear form of equilibrium of a bar in compression and torsion. Izv. Leningr. Politekhn in-ta, Vol. 31.

[22] Oden, J.T. and Martins, J.A.C. (1985) Models and computational methods for dynamic friction phenomena. *Comput. Meth. Appl. Mech. Engrg.*, 52, 527-634.

[23] Pflüger, A. (1950) *Stabilitätsprobleme der Elastostatik*. Springer, Berlin.

[24] Pflüger, A. (1955) Zur Stabilität des tangential gedruckten Stabes. *Z. Angew. Math. Mech.*, 5, 191.

[25] Piccolroaz, A., Bigoni, D. and Willis, J.R. (2006) A dynamical interpretation of flutter instability in a continuous medium. *J. Mech. Phys. Solids*, 54, 2391-2417.

[26] Rice, J.R. (1977) The localization of plastic deformation. In: Koiter, W.T. (Ed.), Theoretical and Applied Mechanics. North-Holland, Amsterdam, 207-220.

[27] Rice, J.R. and Ruina, A.L. (1983) Stability of steady frictional slipping. *J. Appl. Mech.*, 50, 343-349.

[28] Simões, F.M.F. and Martins, J.A.C. (1998) Instability and ill-posedness in some friction problems. *Int. J. Eng. Sci.*36, 1265-1293.

[29] Stribeck, R. (1902) Die wesentlichen Eigenschaften der Gleit- und Rollenlager. *Z. Verein. Deut. Ing.*, 46, 38;39, 1342-1348;1432-1437.

[30] Sugiyama, Y., Katayama, K. and Kinoi, S. (1995) Flutter of a cantilevered column under rocket thrust. *J. Aerospace Eng.*, 8, 9-15.

[31] Sugiyama, Y., Katayama, K., Kiriyama, K. and Ryu, B.-J. (2000) Experimental verification of dynamic stability of vertical cantilevered columns subjected to a sub-tangential force. *J. Sound and Vibration*, 236, 193-207.

[32] Threlfall, D.C. (1977) The inclusion of Coulomb friction in mechanisms programs with particular reference to DRAM. *Metall. Mater. Trans. A*, 13, 475-483.

[33] Ziegler, H. (1953) Linear elastic stability. A critical analysis of methods. *Z. Angew. Math. Phys.*, 4, 89-121.

[34] Ziegler, H. (1956) On the concept of elastic stability. *Advances in Applied Mechanics* , 4, 351-403.

[35] Ziegler, H. (1977) *Principles of structural stability*. Birkhäuser Verlag, Basel und Stuttgart.